GHENT UNIVERSITY

Moisture and heat advection as drivers of global ecosystem productivity

Dominik L. Schumacher
Jessica Keune
Diego G. Miralles

erc

✉ Dominik.Schumacher@UGent.be

OVERVIEW

Approach

Estimation of heat and moisture advection to ecoregions: using a Lagrangian trajectory model (FLEXPART), driven by ERA-Interim reanalysis data, we unravel the origins of heat and moisture. (p. 2)

Rationale & hypotheses

Ecosystem productivity crucially depends on local climate, (p. 3)

local climate depends on advection of heat and (precipitating) moisture,

consequently, ecosystem productivity is driven by heat and moisture advection. (p. 4)

Thus, ecosystem productivity extremes could be caused by anomalous advection of heat and moisture. (p. 5)

Results

For the 5 global ecoregions with strongest interannual GPP variability, all situated in transitional climate regimes, (p. 6)

unusually low GPP is associated with anomalously high amounts of advected heat, yet below-average moisture. (p. 7)

This anomalous advection is a consequence of both (p. 8)

a.) anomalous circulation patterns (generally, a shift from terrestrial toward oceanic source regions occurs),

b.) upwind surface-atmosphere feedbacks, in particular land-atmosphere feedbacks (drought conditions result in enhanced heat yet reduced moisture advection)
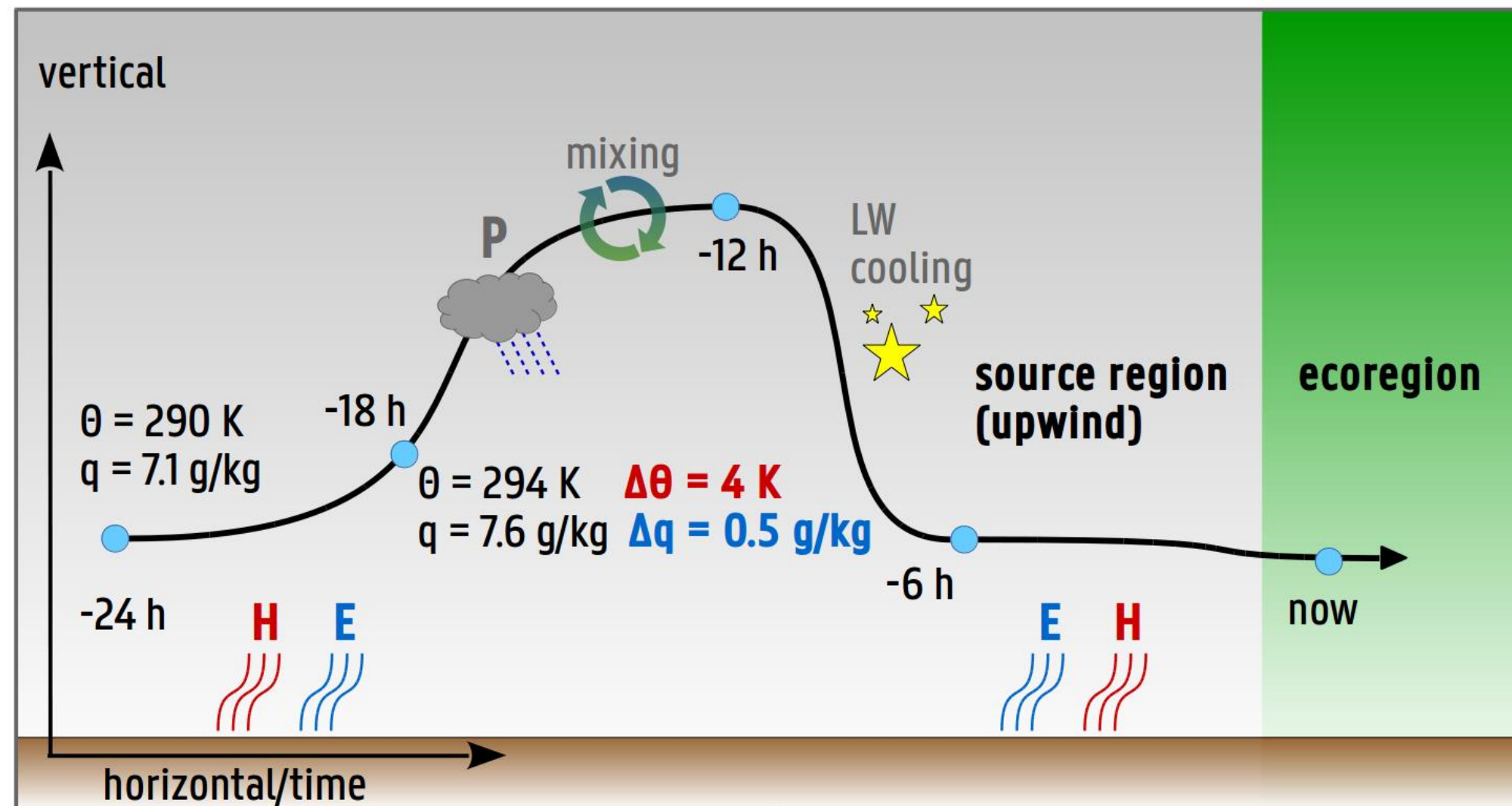
Conclusion

Our results underline

i.   the susceptibility of ecosystems to upwind climatic extremes,

ii.   the role of land-atmosphere feedbacks in these upwind climatic extremes,

iii.   the importance of the latter for the spatiotemporal propagation of ecosystem disturbances.

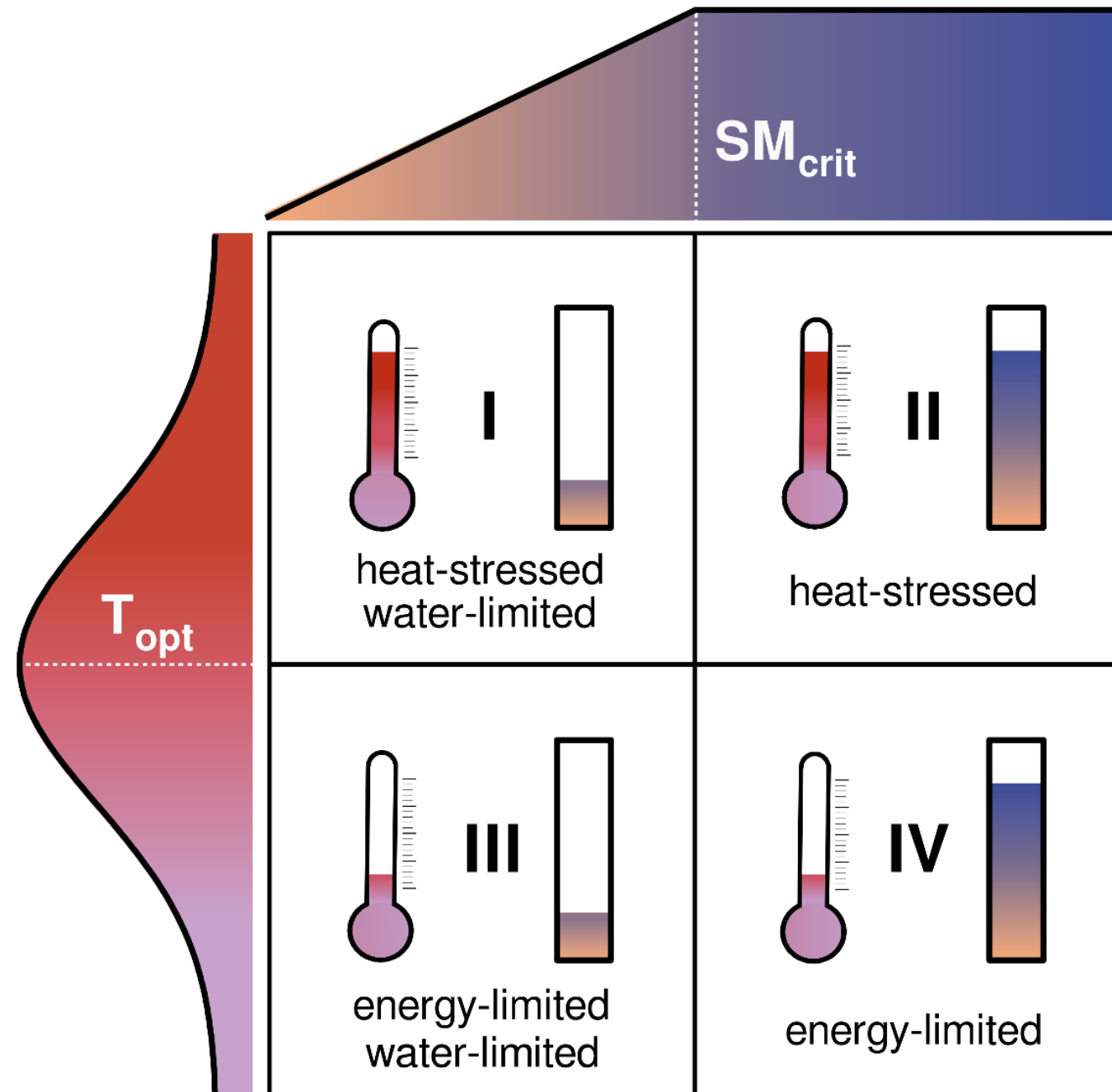# ESTIMATION OF HEAT AND MOISTURE ADVECTION TO ECOREGIONS

In our approach, air parcels residing over ecoregions are followed back in time using a Lagrangian trajectory model, FLEXPART v9.0 (Stohl et al., 2005).

- FLEXPART is driven by 6-hourly ERA-Interim data at 1.0x1.0° horizontal resolution ,
- In FLEXPART, the entire atmosphere is represented by 2 million air parcels around the globe,
- Changes of potential temperature and specific humidity along parcel trajectories are used to infer the origins of heat* and moisture

* in our framework, only diabatic heat origins unrelated to phase changes are considered directly, i.e. surface heating.

ECOSYSTEM PRODUCTIVITY CRUCIALLY DEPENDS ON LOCAL CLIMATE

Schumacher *et al.* (in press)

Ecosystems' optimum temperature (Huang *et al.*, 2019) and a minimum (critical) level of soil moisture (Seneviratne *et al.*, 2010) for which productivity is maximized (T_{opt} and SM_{crit}, respectively).
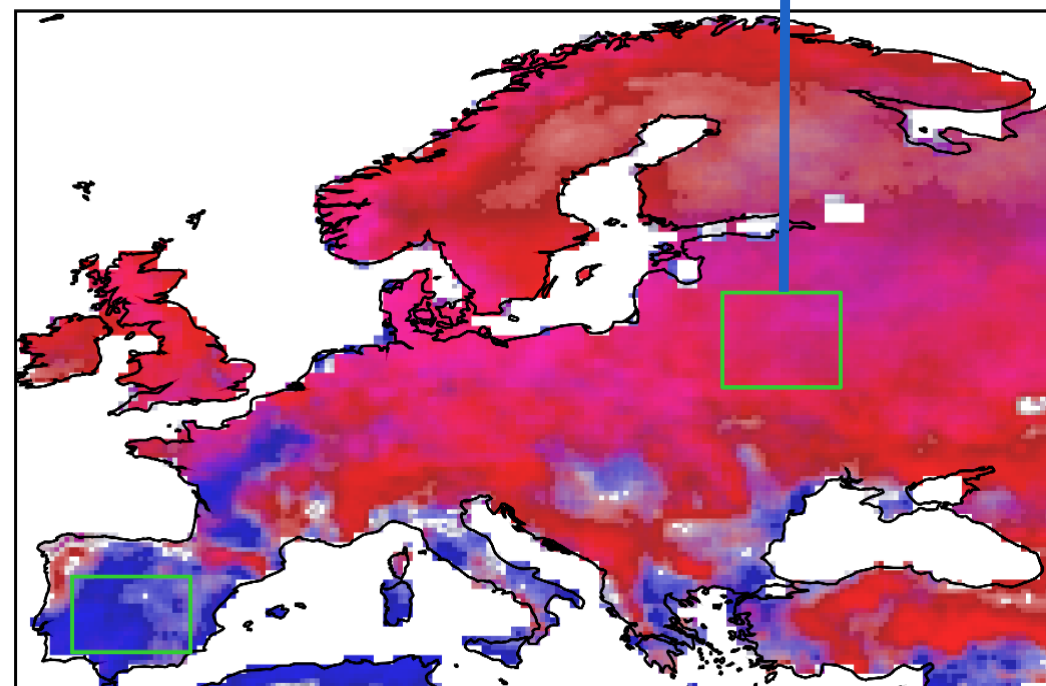
As soon as T_{opt} is exceeded, heat advection is expected to have adverse effects on productivity (heat-stressed types, I and II), whereas higher heat advection is favorable below T_{opt} (energy-limited types, III and IV). Similarly, if soils are below SM_{crit}, productivity is reduced (water-limited types, I and III).

Note that this schematic is a simplification: it does not account for adverse effects of water-logging on productivity (Datta & De Jong, 2002), it illustrates the temperature optimality function as symmetric, and it depicts the soil moisture function as piecewise linear.
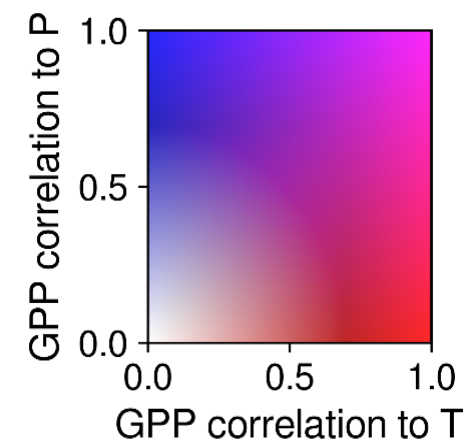
ECOSYSTEM PRODUCTIVITY IS DRIVEN BY HEAT AND MOISTURE ADVECTION

Below: Spearman correlation coefficients between growing-season (FMA) GPP and local temperature T (strong relationships indicated by red), and between GPP and precipitation P (blue), based on 1980–2013.

GPP data obtained from FLUXCOM RS+METEO (Tramontana *et al.* 2016; Jung *et al.*, 2019), T from CRUNCEP v7 (Viovy, 2018), and P from MSWEP v1.1 (Beck *et al.*, 2017).
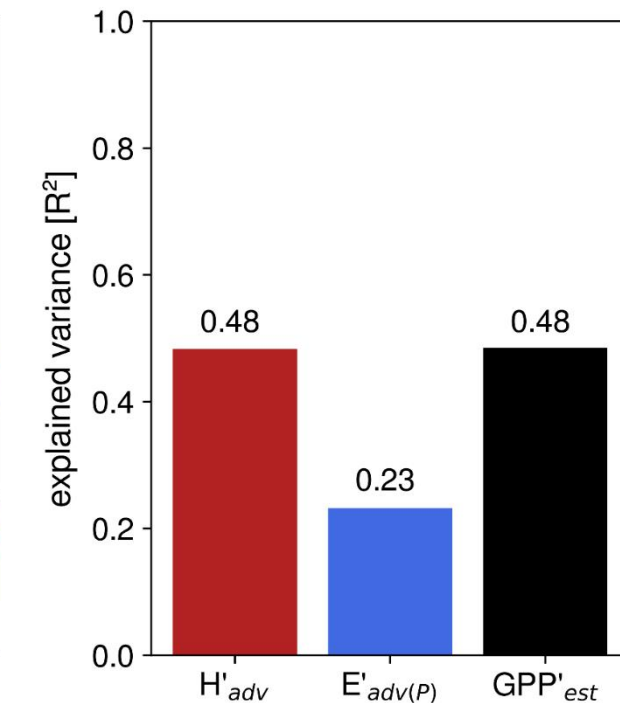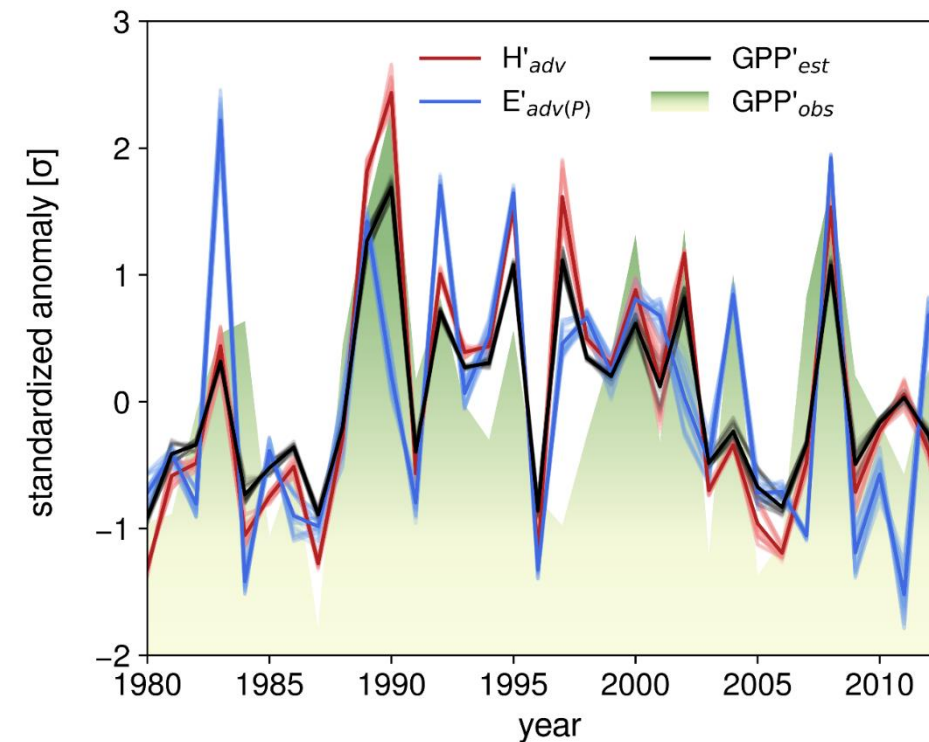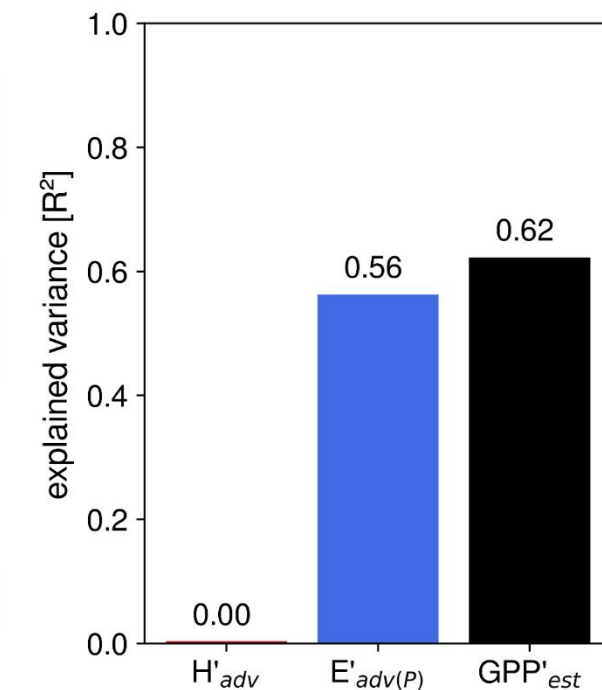
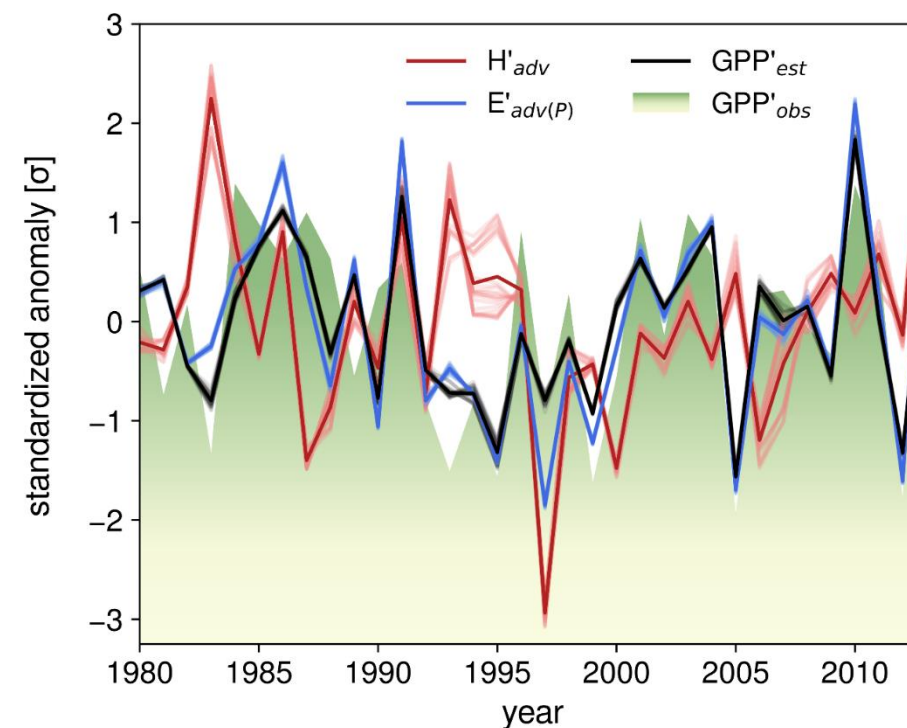**predominantly energy-limited ecoregion**

Schumacher *et al.* (in press)

predominantly water-limited ecoregion

GPP does not covary with advected heat, but more than half of GPP variance can be attributed to advected moisture (see barplot on the right). This is in line with the correlations based on local climatic variables (T, P) shown above.

Standardized anomalies in heat (H'_{adv}) and moisture advection ($E'_{adv(P)}$) and growing-season GPP (GPP'_{obs}). Red and blue bars to the right of the time series denote the ensemble mean–explained variances of GPP'_{obs} by H'_{adv} and $E'_{adv(P)}$, respectively, whereas the black bar denotes the estimated GPP anomaly (GPP'_{est}) obtained using the advection estimates of heat and moisture and a multiple linear regression.
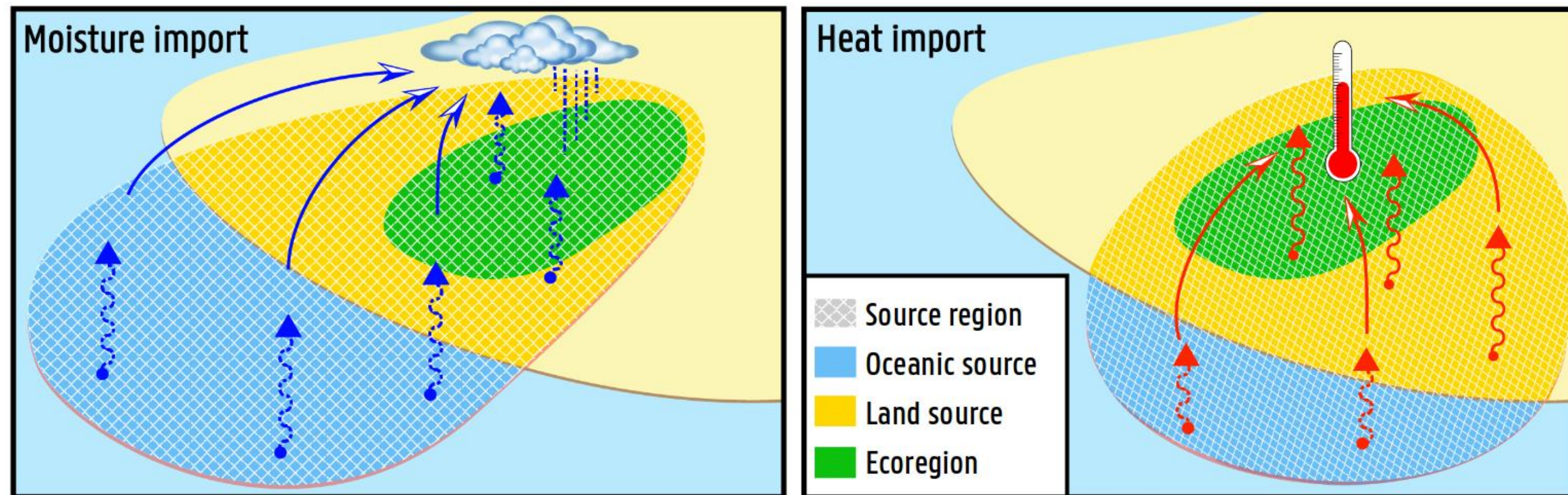
Schumacher *et al.* (in press)

4

ECOSYSTEM PRODUCTIVITY EXTREMES COULD BE CAUSED BY ANOMALOUS HEAT AND MOISTURE ADVECTION

As our atmosphere is flowing continuously, local conditions in ecoregions also depend on the history of advected air:
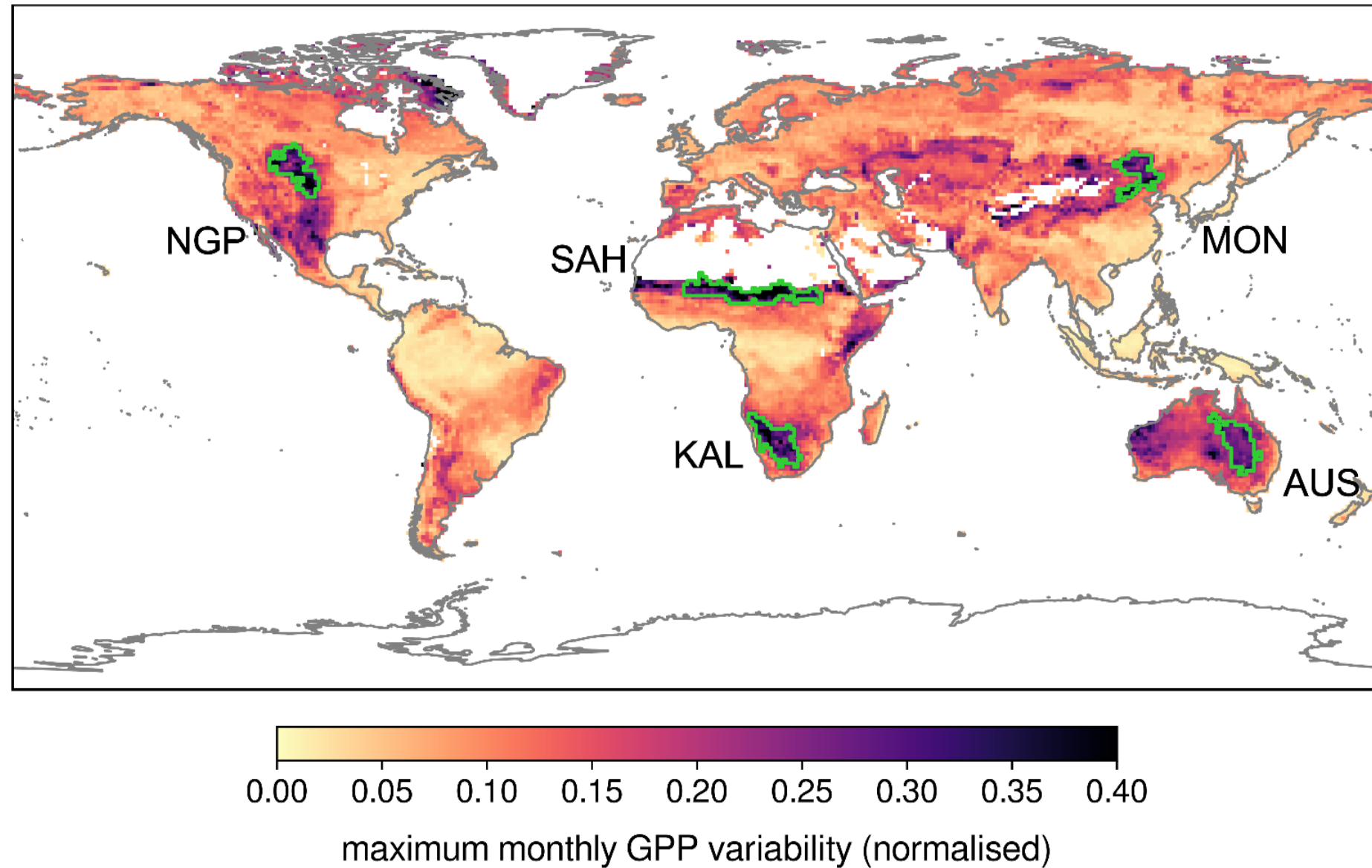
- Where did that air gain moisture in the past, and how much?
- Did some of that moisture rain out *en route* prior to arriving?
- Similarly, where and how much was the air heated by the land surface?

Considering this, and that generally, oceans supply large amounts of moisture to the atmosphere, whereas particularly dry land surfaces tend to heat rather than moisten the atmosphere, *merely a shift in the circulation pattern from oceanic to continental could already result in anomalous advection of heat and moisture to ecoregions (see illustration below).*

Using our heat and moisture tracking framework (p. 2), we investigated this hypothesis for different ecoregions around the globe (p. 6).

Miralles *et al.*, 2016 (modified)

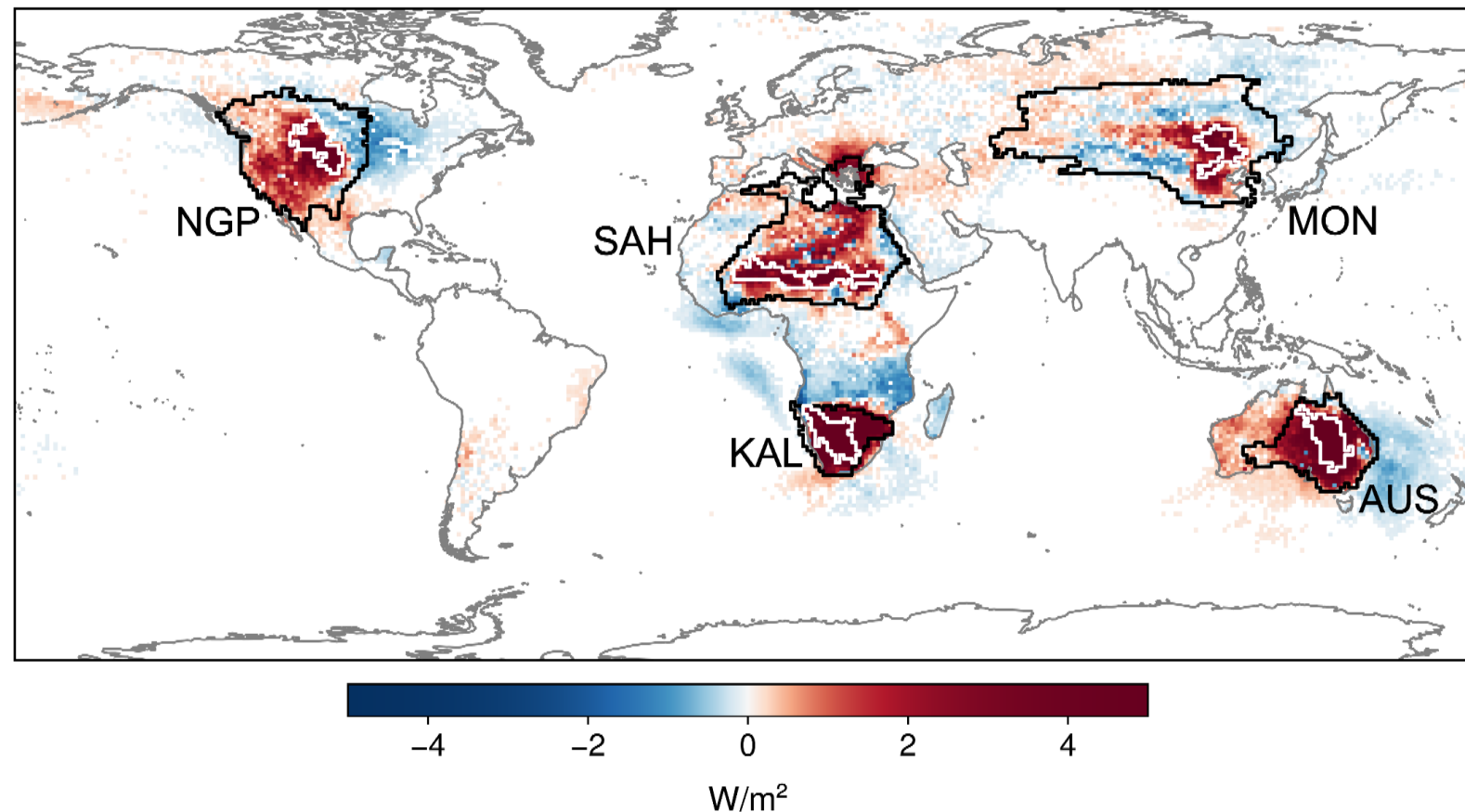# 5 GLOBAL ECOREGIONS WITH STRONGEST INTERANNUAL GPP VARIABILITY

Global hotspots of interannual GPP variability, based on the maximum normalized* monthly standard deviation of GPP (1980–2013).

(* by annual average GPP)

This enables the identification of a 'peak month' per pixel, during which interannual GPP variability is most pronounced.
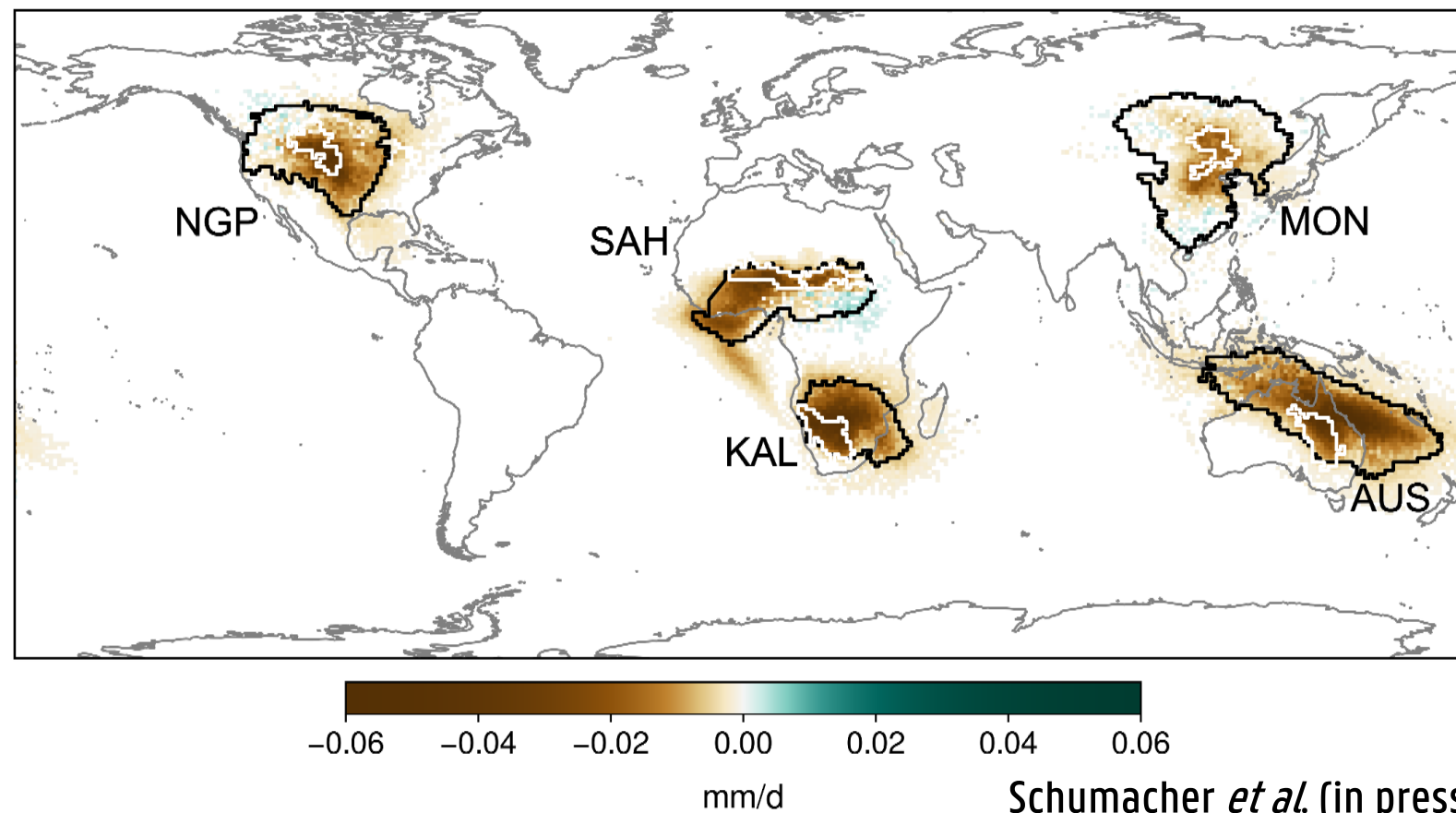
The green contours mark the five ecoregions subject to strong normalized interannual GPP variability (> 0.25) and whose 'peak month' agrees within ± 1 month.

Schumacher *et al.* (in press)

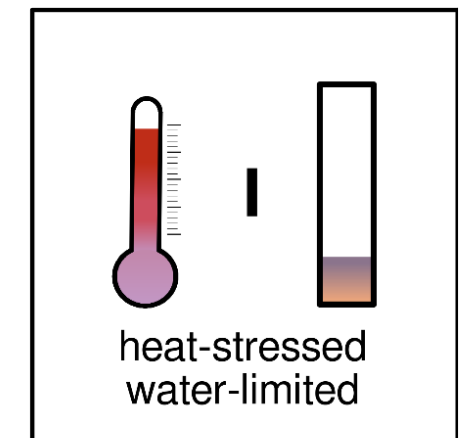# LOW GPP ASSOCIATED WITH HIGH AMOUNTS OF ADVECTED HEAT, YET BELOW-AVERAGE MOISTURE

Advected heat to the five ecoregions (white contours) during low-GPP years, expressed as anomalies for the respective peak month and the two antecedent months. The peak months of NGP, SAH, MON, AUS & KAL are June, August, July; for AUS & KAL, it is February.

Note that white pixels contribute as much during low-GPP years as they do on average; anomalous contributions are indicated by blue and red colors. The climatological mean source regions are delineated using black contours, such that 80% of the average advected heat is accounted for by the smallest possible selection of source pixels.
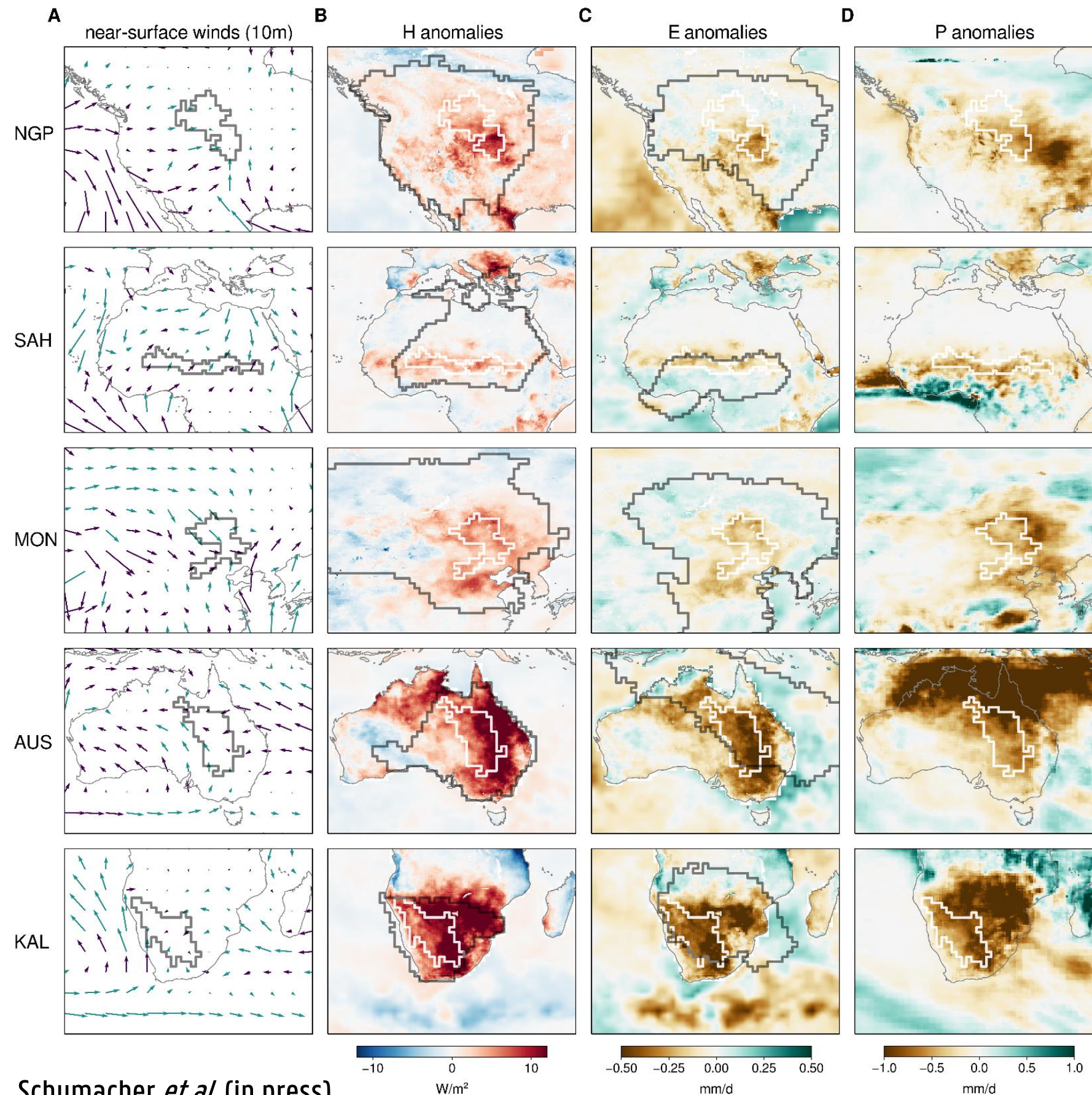
Like the above, but for **advected moisture**.

Our results suggest that all 5 ecoregions, at least during their respective peak month, belong to **type I** on **p. 2**, i.e. are heat-stressed and water-limited.

Unusually low GPP is thus associated with anomalously high (low) amounts of advected heat (moisture).

Schumacher *et al.* (in press)

7

Wind and surface fluxes during low-GPP years

(A) Mean near-surface winds (ERA-Interim; Dee *et al.*, 2010); colored green (purple) indicate that mean wind speeds are higher (lower) than the climatology. Mean wind directions during low-GPP years do not strongly deviate from the overall climatology (not shown).

(B) Surface sensible heat flux anomalies (GLEAM over land; Miralles *et al.*, 2011; Martens *et al.*, 2017, OAFlux over oceans; Yu & Weller, 2007).

(C) Evaporation anomalies (same datasets used as for B)

(D) Precipitation anomalies (MSWEP; Beck *et al.*, 2017).

In all plots, ecoregions are indicated by dark **(A)** or white **(B–D)** contours; for panels **B** and **C**, climatologically advected heat and moisture source regions are visualized by dark contours (as on p. 5).

Our analysis suggests that the advection anomalies (p. 5) are enabled both by changes in circulation patterns and by upwind anomalies in surface evaporation and sensible heat fluxes.

This can be seen well, e.g., in the case of the Australian ecoregion, where heat advection from neighboring land areas to the east is positively anomalous (p. 5) — thanks to extensive positive upwind sensible heat anomalies **(B)** and despite reduced air inflow **(A)**.

Schumacher *et al.* (in press)

GHENT
UNIVERSITY

Atmospheric heat and moisture transport to energy- and water-limited ecosystems

Dominik L. Schumacher
Jessica Keune
Diego G. Miralles

✉ Dominik.Schumacher@UGent.be

erc

REFERENCES

Beck, H.E., A.I.J.M. Van Dijk, V. Levizzani, *et al.* 2017. MSWEP: 3-hourly 0.25° global gridded precipitation (1979–2015) by merging gauge, satellite, and reanalysis data. *Hydrol. Earth Syst. Sci.* **21**: 589–615.

Datta, K.K. & C. De Jong. 2002. Adverse effect of waterlogging and soil salinity on crop and land productivity in north-west region of Haryana, India. *Agric. Water Manag.* **57**: 223–238.

Dee, D.P., S.M. Uppala, A.J. Simmons, *et al.* 2011. The ERA-Interim reanalysis: configuration and performance of the data assimilation system. *Q. J. R. Meteorol. Soc.* **137**: 553–597.

Huang, M., S. Piao, P. Ciais, *et al.* 2019. Air temperature optima of vegetation productivity across global biomes. *Nat.Ecol. Evol.* **3**: 772–779.

Jung, M., S. Koirala, U. Weber, *et al.* 2019. The FLUXCOM ensemble of global land–atmosphere energy fluxes. *Sci. Data* **6**: 74.

Martens, B., D.G. Miralles, H. Lievens, *et al.* 2017. GLEAMv3: satellite-based land evaporation and root-zone soil mois-ture. *Geosci. Model Dev.* **10**: 1903–1925.

Miralles, D.G., T.R.H. Holmes, R.A.M. De Jeu, *et al.* 2011.Global land-surface evaporation estimated from satellite-based observations. *Hydrol. Earth Syst. Sci.* **15**: 453–469.57.

Miralles D.G., R. Nieto, N.G. Mcdowell, *et al.* 2016. Contribution of water-limited ecoregions to their own supply of rainfall. *Environ. Res. Lett.* **11**: 1–12.

Seneviratne, S.I., T. Corti, E.L. Davin, *et al.* 2010. Investigating soil moisture–climate interactions in a changing climate: a review. *Earth Sci. Rev.* **99**: 125–161.

Stohl A., H. Sodemann, S. Eckhardt, *et al.* 2005. The Lagrangian particle dispersion modelFLEXPART The Lagrangian particle dispersion model FLEXPART version 8.2. *Atmos. Chem.Phys.* **5**: 2461–2474.

Tramontana, G., M. Jung, C.R. Schwalm, *et al.* 2016. Pre-dicting carbon dioxide and energy fluxes across globalFLUXNET sites with regression algorithms. *Biogeosciences* **13**: 4291–4313.

Viovy, N. 2018. CRUNCEP version 7 — atmospheric forcing data for the community land model. Research Data Archive at the National Center for Atmospheric Research, Computational and Information Systems Laboratory. Accessed February 17, 2019. http://rda.ucar.edu/datasets/ds314.3/

Yu, L. & R.A. Weller. 2007. Objectively analyzed air–sea heatfluxes for the global ice-free oceans (1981–2005). *Bull. Am.Meteorol. Soc.* **88**: 527–539.